

The impact of the warm outflow in the young (GPS) radio source & ULIRG PKS 1345+12 (4C 12.50)

J. Holt^{1*}, C. N. Tadhunter², R. Morganti^{3,4}, B. H. C. Emonts⁵

¹*Leiden Observatory, Leiden University, PO Box 9513, 2300 RA Leiden, The Netherlands.*

²*Department of Physics and Astronomy, University of Sheffield, Sheffield, S3 7RH, UK.*

³*Netherlands Institute for Radio Astronomy, Postbus 2, 7990 AA Dwingeloo, The Netherlands.*

⁴*Kapteyn Astronomical Institute, University of Groningen, P.O. Box 800, 9700 AV Groningen, The Netherlands*

⁵*Australia Telescope National Facility, CSIRO Astronomy and Space Science, PO Box 76, Epping NSW, 1710, Australia.*

18 August 2010

ABSTRACT

We present new deep VLT/FORS optical spectra with intermediate resolution and large wavelength coverage of the compact radio source and ULIRG PKS 1345+12 (4C 12.50; $z = 0.122$), taken with the aim of investigating the impact of the nuclear activity on the circumnuclear interstellar medium (ISM). PKS 1345+12 is a powerful quasar ($L(\text{H}\beta)_{\text{NLR}} \sim 10^{42} \text{ erg s}^{-1}$) and is also the best studied case of an emission line outflow in a ULIRG. Using the density sensitive transauroral emission lines [S II]4068,4076 and [O II]7318,7319,7330,7331, we pilot a new technique to accurately model the electron density for cases in which it is not possible to use the traditional diagnostic [S II]6716/6731, namely sources with highly broadened complex emission line profiles and/or high ($N_e \gtrsim 10^4 \text{ cm}^{-3}$) electron densities. We measure electron densities of $N_e = (2.94^{+0.71}_{-1.03}) \times 10^3 \text{ cm}^{-3}$, $N_e = (1.47^{+0.60}_{-0.47}) \times 10^4 \text{ cm}^{-3}$ and $N_e = (3.16^{+1.66}_{-1.01}) \times 10^5 \text{ cm}^{-3}$ for the regions emitting the narrow, broad and very broad components respectively. We therefore calculate a total mass outflow rate of $\dot{M} = 8^{+2}_{-3} \text{ M}_{\odot} \text{ yr}^{-1}$, similar to the range estimated for another compact radio source, PKS 1549-79 (Holt et al. 2006). We estimate the total mass in the warm gas outflow is $M_{\text{total}} = (8^{+3}_{-3}) \times 10^5 \text{ M}_{\odot}$ with filling factors of $\epsilon = (4.4^{+1.8}_{-1.5}) \times 10^{-4}$ and $\epsilon = (1.6^{+0.7}_{-0.5}) \times 10^{-7}$ for the regions emitting the broad and very broad components respectively. The total kinetic power in the warm outflow is $\dot{E}_{\text{total}} = (3.4^{+1.5}_{-1.3}) \times 10^{42} \text{ erg s}^{-1}$. Taking the black hole properties published by Dasyra et al. (2006), we find that only a small fraction ($\dot{E}/L_{\text{bol}} = (1.3 \pm 0.2) \times 10^{-3}$) of the available accretion power is driving the warm outflow in PKS 1345+12, which is significantly less than that currently required by the majority of quasar feedback models ($\sim 5\text{--}10\%$ of L_{bol}), but similar to the recent suggestion of Hopkins & Elvis (2010) if a two-stage feedback model is implemented ($\sim 0.5\%$ of L_{bol}). The models also predict that AGN-driven outflows will eventually remove the gas from the bulge of the host galaxy. Our observations show that the visible warm outflow in PKS 1345+12 is not currently capable of doing so. However, it is entirely possible that much of the outflow is either obscured by a dense and dusty natal cocoon and/or in cooler or hotter phases of the ISM. This result is important not just for studies of young (GPS/CSS) radio sources, but for AGN in general.

Key words: ISM: jets and outflows - ISM: kinematics and dynamics - galaxies: active - galaxies: ISM - galaxies: kinematics and dynamics - galaxies: individual: PKS 1345+12 (4C12.50)

1 INTRODUCTION

It has become increasingly clear that the evolution and growth of supermassive black holes and their host galaxy bulges are intricately linked, through the discovery of tight correlations between the bulge and black hole proper-

* E-mail: jholt@strw.leidenuniv.nl

ties (e.g. Ferrarese & Merritt 2000; Gebhardt et al. 2000; Tremaine et al. 2002; Marconi & Hunt 2003; Benson et al. 2003). However, whilst the observed correlations become better constrained, the physical processes responsible are still not understood (e.g. Cattaneo et al. 2009) with both AGN feedback (e.g. Silk & Rees 1998) and starburst supernova feedback (e.g. Wild et al. 2010) providing plausible outflow driving mechanisms.

A number of theoretical models have successfully reproduced the observed correlations by including AGN feedback in which the rapidly accreting black hole dissipates energy into the surrounding ISM by driving powerful outflows, which halt further accretion and star formation (e.g. Silk & Rees 1998; Fabian 1999; Di Matteo et al. 2005; Springel et al. 2005). Currently, these models require a significant amount of the accretion energy to be mechanically coupled to the ISM ($\sim 5\text{--}10\%$ of L_{bol} ; e.g. Di Matteo et al. 2005; Tremaine et al. 2002; Springel et al. 2005; Kurosawa et al. 2009; Booth & Schaye 2009), although recent work by Hopkins & Elvis (2010) suggests that if a two-stage feedback model is implemented, the initial energy requirement may be a factor of 10 lower.

Over the last decade, the signatures of such mechanical AGN feedback (outflows) have been observed in Compact Steep Spectrum (CSS; $D_{\text{radio}} < 15\text{ kpc}$) and GigaHertz-Peaked Spectrum (GPS; $D_{\text{radio}} < 1\text{ kpc}$) radio sources, both in the warm (e.g. optical emission line outflows; e.g. Holt et al. 2008) and cold (e.g. HI absorption line outflows; e.g. Morganti et al. 2005) gas. In the infra-red, emission line outflows have also recently been discovered in ULIRGs (Spoon & Holt 2009).

CSS and GPS radio sources are ideal objects for studying the effects of AGN feedback as they are believed to be young, recently triggered radio-loud AGN (see O’Dea 1998 for an extensive review of these sources). The similarities in scale of the AGN, compact radio source and the dense circumnuclear ISM mean that interactions will be strong and readily detectable. In 2006, Holt et al. performed a detailed study of the outflow in the southern compact flat-spectrum radio source PKS 1549-79, deriving a mass outflow rate of $0.12 < \dot{M} < 12 M_{\odot} \text{ yr}^{-1}$ and a kinetic power of $5.1 \times 10^{40} < \dot{E} < 5.1 \times 10^{42} \text{ erg s}^{-1}$, which accounts for only a small fraction of the available accretion energy in this source ($10^{-6} < \dot{E}/L_{\text{Edd}} \sim 10^{-4}$). However, due to the large uncertainties in the measured density, it was impossible to derive these crucial parameters more accurately.

The young radio galaxy PKS 1345+12 (GPS; $D_{\text{radio}} \sim 350\text{ pc}$; Stanghellini et al. 1993) is a prime object for AGN feedback studies as it contains all of the signatures of a recently triggered powerful¹ AGN currently shedding its natal cocoon. Fast outflows (up to $\sim 2000\text{ km s}^{-1}$) are detected in both the warm and cold circumnuclear gas (e.g. Holt et al. 2003; H03 hereafter, Morganti et al. 2005). The host galaxy is highly disturbed; the double nucleus (sepa-

rated by ~ 1.8 arcsec or 4.3 kpc) is embedded in an extended, asymmetric halo with clear evidence for extended, distorted morphology (e.g. Smith & Heckman 1989), suggesting PKS 1345+12 has been involved in a major merger in its recent past. In addition, prodigious star formation activity is observed. PKS 1345+12 has a substantial far-IR excess ($L_{\text{FIR}} = 1.7 \times 10^{12} L_{\odot}$, Evans et al. 1999), qualifying this source as an ultra-luminous IR galaxy (ULIRG). Furthermore, significant young stellar populations have been detected in the halo, both in the diffuse emission (Tadhunter et al. 2005) and in a number of young Super Star Clusters (SSCs; Rodriguez Zaurin et al. 2007). Hence, detailed studies of the outflow in PKS 1345+12 are important for a number of classes of objects (powerful AGN, GPS/CSS radio galaxies and ULIRGs) with the outflow being the best studied example of an optical emission line outflow in a ULIRG.

A key parameter for determining the importance of the nuclear outflows in terms of galaxy evolution is the electron density of the gas, which allows the calculation of the mass outflow rate and kinetic power of the outflow. Traditionally, gas densities have been successfully derived for many AGN using the [S II]6715,6731 doublet, which requires an accurate measurement of the ratio between the two lines in the blend. However, sources with highly complex emission line profiles can preclude accurate modelling of the [S II] doublet. In the case of PKS 1345+12, the velocity widths and shifts of the broader components are comparable to the separation of the doublet. Hence, whilst total fluxes in each component can be established, it is often not possible to determine how much of the emission in each component originates from each line in the blend. In addition, our previous study of PKS 1345+12 (H03) has suggested that the densities in the nuclear regions of young radio-loud AGN are high ($N_e > 4 \times 10^3 \text{ cm}^{-3}$), and may be high enough to be outside the range of densities to which the [S II] diagnostic is sensitive ($N_e = 10^2\text{--}10^3 \text{ cm}^{-3}$).

In this paper, we present new, high quality VLT/FORS2 spectra of PKS 1345+12, which are both deeper, and cover a wider wavelength range, than our previous WHT/ISIS spectra presented in H03. The new spectra now include further density sensitive emission lines, namely the transauroral [S II]4068,4076 and [O II]7318,7319,7330,7331 lines, to pilot a new technique to measure the electron density of the circumnuclear emission line gas. Consequently, we calculate for the first time the mass outflow rate and kinetic power of the optical (warm) outflow in a young radio-loud AGN and ULIRG.

Throughout this paper we assume the following cosmology: $H_0 = 71 \text{ km s}^{-1}$, $\Omega_0 = 0.27$ and $\Omega_{\Lambda} = 0.73$.

2 OBSERVATIONS AND DATA REDUCTION

We have obtained new, deep long-slit optical spectroscopic observations of PKS 1345+12 in service mode on 22nd March 2007. Using FORS2 on the ESO Very Large Telescope (VLT) in LSS mode with GRIS-600B+22, GRIS-600RI+19 and GRIS-600Z+23, and a 1.3 arcsec slit, we obtained spectra along PA 160 with large spectral coverage (rest frame: 3200–9200 Å).

The data were reduced in the usual way (bias subtraction, flat fielding, cosmic ray removal, wavelength calibration, flux calibration) using the standard packages in IRAF. The two-dimensional spectra were also corrected for spa-

¹ $L(\text{H}\beta)_{\text{NLR}} \sim 10^{42} \text{ erg s}^{-1}$; c.f. the SDSS DR7 quasar catalogue (Schneider 2010) which includes $\text{H}\beta$ luminosities split into the NLR and BLR components. The NLR $\text{H}\beta$ luminosity of PKS 1345+12 (we do not detect the BLR) is well above the mean value of NLR $\text{H}\beta$ luminosities in quasars, making it a very powerful AGN. This is also evident in its large [O III] luminosity.

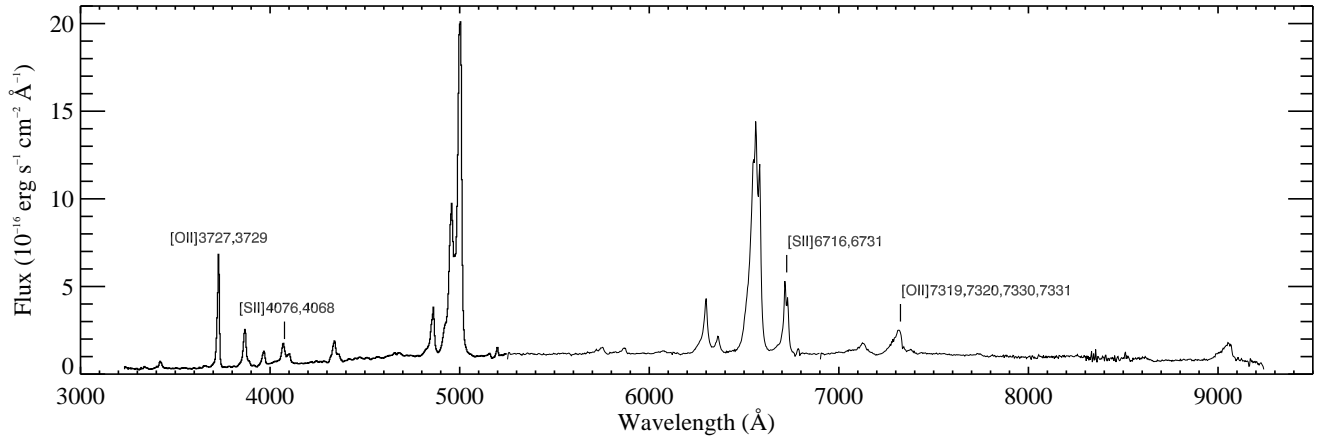


Figure 1. Rest frame spectrum of the nuclear aperture of PKS 1345+12. The key density diagnostic emission lines used in this paper are highlighted.

tial distortions of the CCD. The final wavelength calibration accuracy, calculated using the standard error on the mean deviation of the night sky emission line wavelengths from published values (Osterbrock et al. 1996) was 0.281, 0.112 and 0.035 Å in the blue, red and z bands respectively. The spectral resolution of the night sky emission lines was $6.65 \pm 0.16 \text{ Å}$, $7.15 \pm 0.41 \text{ Å}$ and $7.02 \pm 0.37 \text{ Å}$ in the blue, red and z bands respectively.

Comparison of several spectral photometric standard stars taken with a wide slit (5 arcsec) gave a relative flux calibration accurate to ± 5 per cent. This accuracy was confirmed by comparison to our earlier data (H03). A further standard star was observed with a narrow slit, matched to that used to observe PKS 1345+12, to correct for atmospheric absorption features (e.g. A and B bands at ~ 7600 and $\sim 6800 \text{ Å}$ respectively).

The main aperture used was the nuclear aperture – 1.5 arcsec wide, centred on the nuclear continuum emission, and is shown in Figure 1. Before modelling the emission lines in the nuclear aperture, the continuum was modelled and subtracted, a step which has been shown to be crucial in the modelling of the broader, blueshifted components of the emission lines (e.g. H03, Holt et al. 2006, 2008, 2009). Our continuum model comprised a nebular continuum (see e.g. Dickson et al. 1995) and a modelled stellar continuum following the methods of e.g. Tadhunter et al. (2005); Holt et al. (2006, 2007).

The spectra were extracted and analysed using the STARLINK packages FIGARO and DIPSO.

3 RESULTS

In this paper, our analysis focusses on the density of the emission line gas in the circumnuclear regions. We will therefore discuss only the relevant density diagnostic lines ([O II] and [S II]; see Figure 1) and refer the reader to H03 for a detailed discussion of the other strong nuclear emission lines in this source.

3.1 Emission line modelling

The nuclear emission lines in PKS 1345+12 are strong, characterised by highly broadened profiles with strong blue wings. A detailed study of the emission line spectrum of the nucleus of PKS 1345+12 showed that the emission lines required a minimum of 3 Gaussian components to model them (H03). Here, we implement the model derived by H03 for [O III] 4959,5007 (hereafter the [O III] model). This model comprises²:

- (i) a narrow component, FWHM $340 \pm 23 \text{ km s}^{-1}$ at the systemic velocity ($z = 0.12174 \pm 0.00002$);
- (ii) a broad component, FWHM $= 1255 \pm 12 \text{ km s}^{-1}$; blueshifted by $402 \pm 9 \text{ km s}^{-1}$ with respect to the narrow component (note H03 refer to this component as ‘intermediate’);
- (iii) a very broad component, FWHM $= 1944 \pm 65 \text{ km s}^{-1}$, blueshifted by $1980 \pm 36 \text{ km s}^{-1}$ with respect to the narrow component (note H03 refer to this component as ‘broad’).

Figure 2 shows the [O III] model applied to the [O II] 7319,7320,7330,7331 blend, which we have modelled as a doublet (i.e. one line centred at $\sim 7320 \text{ Å}$ and one line centred at $\sim 7330 \text{ Å}$), with each line comprising three distinct emission line components. The [O III] model gives a good fit to the blend. In addition, the [O III] model provides reasonable fits to all of the other lines ([S II] 6716,6731, [O II] 3727,3729 and [S II] 4068,4076). Note that [O II] 3727,3729 and [S II] 4076,4086 were also modelled as single lines, for a number of detailed line-fitting reasons. The measured line ratios are plotted on the density diagnostic diagram in Figure 3.

Note that H03 found that the [O III] model did not model all of the emission lines perfectly. This included [S II] 6716,6731 which was best fit by a model with slightly different FWHM and velocity shifts for the broad and very broad components. Furthermore, for all models to [S II], the

² The notations narrow, intermediate, broad and very broad follow the kinematical component definitions of Holt et al. (2008).

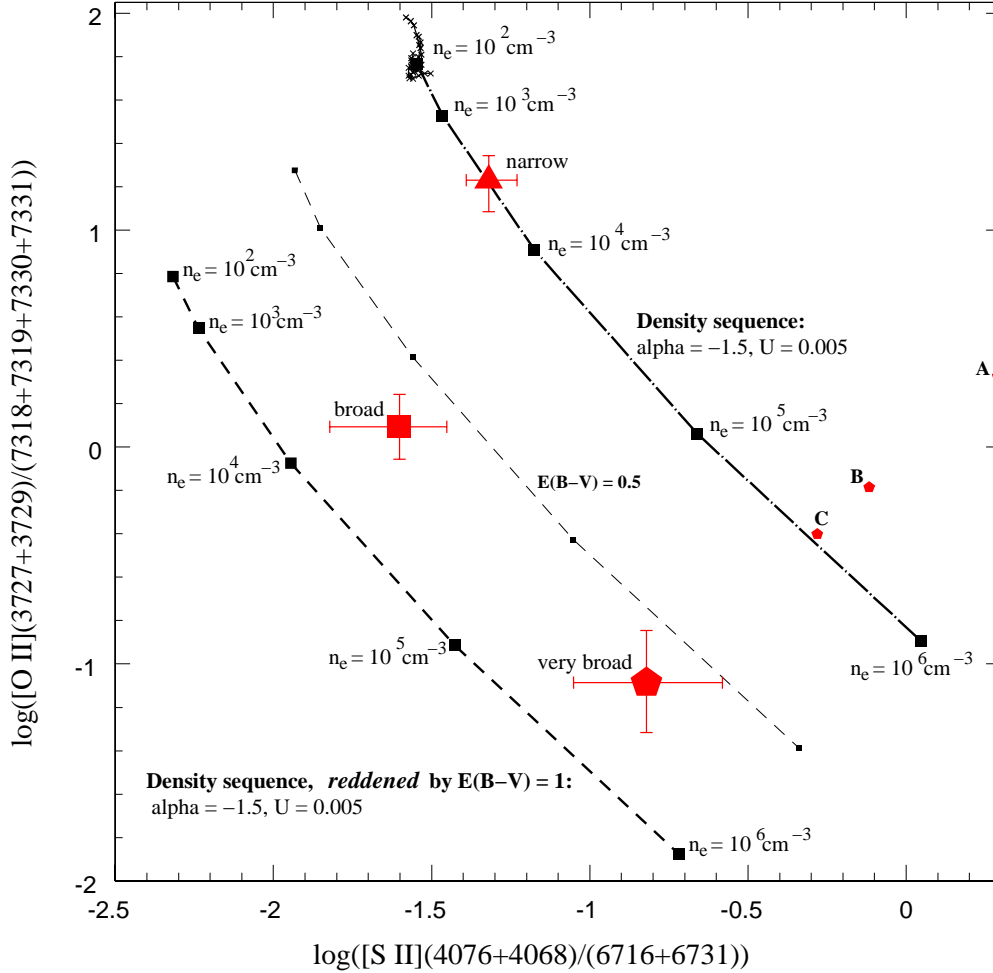


Figure 3. A diagnostic diagram using all of the key density diagnostic lines. The crosses joined by solid lines are the simple, optically thick AGN-photoionisation generated using the multi-purpose photoionisation code MAPPINGS. The models are sequences in ionisation parameter, U , for optically thick single-slab power-law ($F_\nu \propto \nu^\alpha$) for spectral index $\alpha = -1.0, -1.5, -2.0$ and an electron density of $n_e = 100 \text{ cm}^{-3}$. Also plotted is a density sequence (squares joined by a dot-dashed line) which has a constant power law ($\alpha = -1.5$) and ionisation parameter ($U = 0.005$) with electron densities of $n_e = 10^2, 10^3, 10^4, 10^5$ and 10^6 cm^{-3} . Finally, the squares joined by the dashed lines represent the same density sequence but *reddened* by $E(B-V) = 0.5$ (faint line) and $E(B-V) = 1.0$ (bold line) using the Seaton (1979) extinction law. The large red points are the measured (i.e. without reddening correction) data: narrow (triangle), broad (square) and very broad (pentagon). In addition, the small red pentagons give the position of the very broad component after applying various reddening corrections: A: $E(B-V) = 1.44$, B: $E(B-V) = 0.92$ and C: $E(B-V) = 0.7$. See the text for a discussion of the various $E(B-V)$ values.

intensity ratios for the components needed to be fixed to ensure that they were within the permitted range ($0.44 < [\text{S II}]6716/6731 < 1.42$) and that the fit was physically viable. The main reason for the difficulty in modelling $[\text{S II}]$ was that the widths and shifts of the broader components are comparable to the separation of the doublet. We find the situation unchanged for the new VLT data. For the new diagnostic, only the total flux in each kinematic component is required. By removing the need for an accurate ratio between the two lines in the $[\text{S II}]6716,6731$ doublet, the $[\text{O III}]$ model can provide a good model to the doublet. To test the robustness of our fit, in addition to our ‘free intensity’ $[\text{O III}]$ model to the $[\text{S II}]6716,6731$ blend, we have also tried forcing the component ratios so all lie within the range quoted above.

These give errors of 6%, 9% and 12% on the total fluxes in the narrow, broad and very broad components respectively.

3.2 The electron density

A key parameter for determining the importance of the nuclear outflows in terms of galaxy evolution is the electron density of the gas. As discussed above, due to the highly complex emission line profiles in the nuclear regions of PKS 1345+12, it was not possible to measure the density using the $[\text{S II}]6715,6731$ doublet. Here, we pilot a new technique based on the transauroral $[\text{S II}]$ and $[\text{O II}]$ lines.

Figure 3 shows a new diagnostic diagram constructed for the transauroral density diagnostic

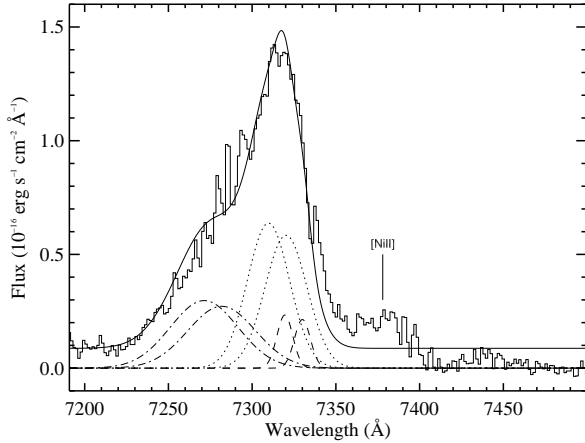


Figure 2. The [O II]7319,7320,7330,7331 emission line blend. The faint solid line is the observed spectrum, the bold line is the overall fit, the dashed lines are the narrow components, the dotted lines are the broad components and the dot-dashed lines are the very broad components. The vertical line marks the position of [Ni III]7378 in the red wing of the [O II] blend.

lines [O II]3727/(7318+7319+7330+7331) and [S II](4068+4076)/(6716+6731). As discussed above, diagnostics relying only on the total flux in each emission line component in each blend bypasses the issue faced with the [S II]6716/6731 ratio. In addition, as demonstrated by the reddening tracks plotted on Figure 3, whilst the lines span a large range of wavelengths, it is not necessary to perform separate reddening corrections. The diagnostic is also not sensitive to the details of the ionisation model.

From Figure 3, we obtain electron densities of $N_e = (2.94^{+0.71}_{-1.03}) \times 10^3 \text{ cm}^{-3}$, $N_e = (1.47^{+0.60}_{-0.47}) \times 10^4 \text{ cm}^{-3}$ and $N_e = (3.16^{+1.66}_{-1.01}) \times 10^5 \text{ cm}^{-3}$ for the narrow, broad and very broad components respectively. These densities are much higher than the original estimates based on [S II]6716/6731 and suggest that, even without the problems faced modelling the blend, the diagnostic would not give accurate densities as the measured densities are beyond the range the [S II]6716/6731 ratio is sensitive to.

Further diagnostic lines sensitive to higher densities are [Cl III]5518,5534 (sensitive to $\sim 10^4 \text{ cm}^{-3}$) and [Ar IV]4713,4742 (sensitive to $10^4 - 10^5 \text{ cm}^{-3}$). Both of these doublets have been observed in Cygnus A, although they are weak (Tadhunter et al. 1994). Neither doublet was detected in the original WHT/ISIS spectrum of H03. In these data, we detect very faint [Ar IV]4713,4742 although there is no evidence of [Cl III] emission (see Figure 4). The detection of [Ar IV] further supports the high densities measured in PKS 1345+12. In addition, we detect [S III]9069 (Figure 1) which also has a high critical density ($1.2 \times 10^6 \text{ cm}^{-3}$).

3.3 Reddening

As discussed above, PKS 1345+12 is known to harbour a dense and dusty circumnuclear cocoon. The level of reddening in the optical spectrum was investigated in detail by H03, using three separate techniques: Balmer line ra-

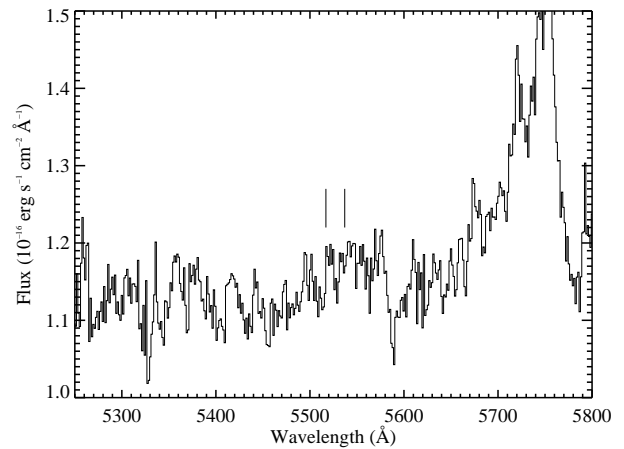
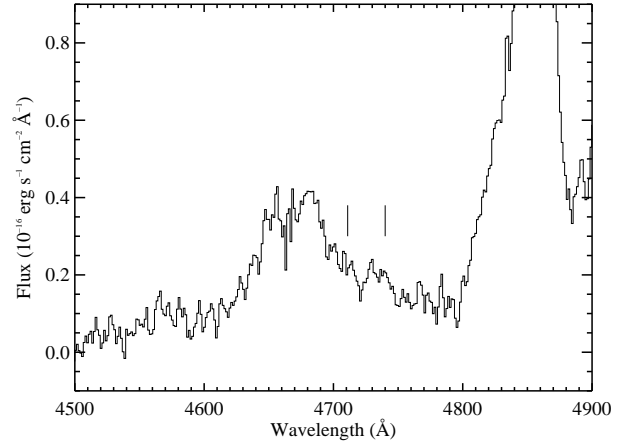


Figure 4. The regions of the nuclear rest frame spectra in which the higher density sensitive lines [Ar IV]4713,4742Å (top panel) and [Cl III]5518,5534Å (bottom panel) would be located. Vertical lines mark the wavelengths of the lines. A weak component of [Ar IV]4742 is observed (top panel), but we do not detect any of the other lines.

tios (e.g. $H\alpha/H\beta$); comparison of the optical results with published near-IR data ($P\alpha/H\beta$) and consideration of the nebular continuum as part of the SED modelling. The reddening results of H03 are summarised in Table 1. Here, we further investigate the reddening using our density diagnostic (Figure 3).

In addition to electron density sequences, a number of reddening ($E(B-V)$) sequences, derived using the Seaton (1979) extinction law, are also plotted on Figure 3. From Figure 3, the reddening is estimated to be $E(B-V) = 0.0 \pm 0.1$, $E(B-V) = 0.7 \pm 0.2$ and $E(B-V) = 0.7 \pm 0.2$ for the narrow, broad and very broad components respectively. For the narrow component, this is consistent with the results of H03 although the $E(B-V)$ values for the broad and very broad components are somewhat higher and lower than those derived by H03 respectively.

In terms of line ratios, a ‘cleaner’ method would be to use unblended line combinations, such as $P\alpha/H\beta$. H03 attempted to use $P\alpha/H\beta$ to improve the reddening estimate but issues such as differing components and uncertainties about possible slit losses between the optical and near-IR

Table 1. Reddening values and emission line data. Columns are: (a) Quantity, where: $H\alpha/H\beta$ is the flux ratio between the measured values of $H\alpha$ and $H\beta$; $E(B-V)(H\alpha/H\beta)$ is the $E(B-V)$ value calculated using the $H\alpha/H\beta$ ratio and the standard interstellar extinction curve from Seaton (1979); $F_{H\beta}$ is the reddening corrected $H\beta$ line flux (10^{-15} erg s $^{-1}$ cm $^{-2}$); $L_{H\beta}$ is the rest frame $H\beta$ luminosity (10^{40} erg s $^{-1}$); $E(B-V)(\text{limits})$ gives the lower limits on the $E(B-V)$ value derived for the broad and very broad components by H03; $E(B-V)(\text{diagnostic})$ is the $E(B-V)$ value derived from the diagnostic diagram in Figure 3; (b) value of particular quantity for the narrow component; (c) uncertainty for narrow component; column pairs (d) and (e) and (f) and (g) are as for (b) and (c) but for the broad and very broad components respectively.

^a derived from considerations of the nebular continuum (H03). ^b derived from $H\alpha/H\beta$ using the model to the $H\alpha, [N \text{ II}]$ blend which gives the lowest possible flux in $H\alpha$ (H03). ^c derived using the $E(B-V)$ values given in row 2 of this Table. ^d luminosity from H03 updated to the cosmology used in this paper. ^e derived using the new (VLT) $H\beta$ fluxes and $E(B-V)(\text{diagnostic})$ values.

(a)	narrow (b)	Δ (c)	broad (d)	Δ (e)	very broad (f)	Δ (g)
Taken from H03						
$H\alpha/H\beta$	3.32	0.33	5.26	0.28	18.81	4.74
$E(B-V)(H\alpha/H\beta)$	0.06	0.05	0.42	0.10	1.44	0.50
$E(B-V)(\text{limits})$			$>0.3^a$		$>0.92^b$	
$F_{H\beta}$ (10^{-15} erg s $^{-1}$ cm $^{-2}$) ^c	0.72	0.06	8.8	0.4	43	10
$L_{H\beta}$ (10^{40} erg s $^{-1}$) ^d	2.7	0.2	33	2	160	40
This paper						
$E(B-V)(\text{diagnostic})$	0.0	0.1	0.7	0.2	0.7	0.2
$F_{H\beta}$ (10^{-15} erg s $^{-1}$ cm $^{-2}$) ^e	1.1	0.2	41	5	15	4
$L_{H\beta}$ (10^{40} erg s $^{-1}$) ^e	4.3	0.7	155	18	56	15

data proved difficult. We have since obtained the unpublished near-IR spectrum of Veilleux (priv. comm.) in an attempt to model Pa α with our three component [O III] model. Whilst we can obtain a good fit, it is no better than the original two component model, and still does not help with regards to the issue of slit losses.

Given the uncertainties regarding the degree of reddening, H03 attempted to derive limits for the reddening using a more indirect technique. By generating nebular continua with various $E(B-V)$ values, H03 set a lower limit on the reddening in the broad component, the component which dominates the flux in the nebular continuum. This technique gave a lower limit of $E(B-V) > 0.3$ for the broad component, which is consistent with all reddening estimates for this component.

Given the uncertainties in the reddening estimates, we have also plotted the reddening corrected line ratios for the very broad component using various $E(B-V)$ values, in order to assess how the degree of reddening affects our derived density. For this exercise we have chosen three $E(B-V)$ values:

- (i) point A: $E(B-V) = 1.44$; the value derived by H03 using $H\alpha/H\beta$;
- (ii) point B: $E(B-V) = 0.92$; the lower limit for the reddening derived by H03;
- (iii) point C: $E(B-V) = 0.7$; the value derived by our diagnostic diagram.

As can be seen from Figure 3, whilst the poorly constrained

$E(B-V)$ value will affect the reddening corrected $H\beta$ luminosity, it has little effect on the derived electron density. We therefore conclude that the electron densities derived using this technique are robust.

4 DISCUSSION

4.1 How important is the warm outflow in PKS 1345+12?

In recent years AGN feedback, in the form of quasar-driven outflows, has been relied upon to explain a number of observed relations, such as the close correlation between black hole mass and the galaxy bulge properties (e.g. Silk & Rees 1998; Fabian 1999; Ferrarese & Merritt 2000; Gebhardt et al. 2000; Tremaine et al. 2002; Marconi & Hunt 2003; Di Matteo et al. 2005; Kurosawa et al. 2009; Booth & Schaye 2009) and the high end shape of the galaxy luminosity function (e.g. Benson et al. 2003). Currently, the majority of AGN feedback models require a significant amount of the available accretion energy to power the outflows ($\sim 5\text{--}10\%$; e.g. Di Matteo et al. 2005; Springel et al. 2005; Booth & Schaye 2009; Kurosawa et al. 2009) although this has recently been brought into question, with much lower energy injection required if a two-stage feedback model is implemented ($\sim 0.5\%$ of L_{bol} ; Hopkins & Elvis 2010).

PKS 1345+12 provides an ideal test case for investi-

gating the impact of AGN feedback in the early stages of AGN evolution. Clearly currently still undergoing a major merger/interaction (c.f. double nucleus within a single diffuse halo with a number of tidal features and evidence for recent star formation), the small, recently triggered radio jets are currently expanding through a dense natal cocoon of gas and dust (c.f. large electron densities and reddening, high X-ray and HI absorbing columns). Our optical spectra reveal clear signatures of AGN driven outflows in the strong, highly broadened and blueshifted optical emission lines. Whilst the outflows are fast, it is important to combine this kinematic information with other properties, such as the gas density, to determine the key parameters for understanding the importance of AGN feedback – the mass outflow rate and the kinetic power.

Following the derivation in Holt et al. (2006), the mass outflow rate for a spherical outflow can be expressed as:

$$\dot{M} = \frac{3L(H\beta)m_p v_{out}}{N\alpha_{H\beta}^{eff} h\nu_{H\beta} r} \quad (1)$$

where $L(H\beta)$ is the $H\beta$ luminosity, m_p is the mass of the proton, v_{out} the outflow velocity, N is the electron density of the gas, $\alpha_{H\beta}^{eff}$ is the effective $H\beta$ recombination coefficient (see Osterbrock 1989), $\nu_{H\beta}$ the frequency of $H\beta$, h the Planck constant and r is the radius of the spherical volume.

We take $H\beta$ luminosities measured from our new VLT spectra, modelled with the [O III] model of H03, and corrected for extinction using the E(B-V) values derived by our diagnostic diagram (Figure 3) and the Seaton (1979) extinction law, all of which are summarised in Table 1. In our currently adopted cosmology, these are: $L(H\beta)_N = (4.3 \pm 0.7) \times 10^{40}$ erg s⁻¹; $L(H\beta)_B = (1.55 \pm 0.18) \times 10^{42}$ erg s⁻¹ and $L(H\beta)_{VB} = (5.6 \pm 0.15) \times 10^{41}$ erg s⁻¹. The rest frame outflow velocities (v_{out}) are $v_B = 402 \pm 9$ km s⁻¹ and $v_{VB} = 1980 \pm 65$ km s⁻¹. Using our new diagnostic tool (Figure 3), we measure electron densities of $N_e = (2.94^{+0.71}_{-1.03}) \times 10^3$ cm⁻³, $N_e = (1.47^{+0.60}_{-0.47}) \times 10^4$ cm⁻³ and $N_e = (3.16^{+1.66}_{-1.01}) \times 10^5$ cm⁻³ for the narrow, broad and very broad components respectively. If we assume case B recombination theory for an electron temperature $T = 10,000$ K and that the outflow is spherical, with a radius half of the diameter of the [O III] emission line region imaged by HST ACS (Batcheldor et al. 2007) (i.e. 7.5 milli-arcseconds or $r = 162$ pc for our cosmology), we calculate mass outflow rates of $\dot{M} = 7.1^{+2.0}_{-2.6}$ M_⊙ yr⁻¹ and $\dot{M} = 0.6^{+0.3}_{-0.2}$ M_⊙ yr⁻¹ in the two outflowing components respectively, with a total mass outflow rate of $\dot{M} = 7.7^{+2.2}_{-2.9}$ M_⊙ yr⁻¹. This estimate is comparable to the range of mass outflow rates calculated for another young radio source, PKS 1549-79 (H06) but lies between the mass outflow rates estimated for the NLR of Seyferts (0.1-1.0 M_⊙ yr⁻¹; e.g. Veilleux et al. 2005) and the much larger neutral outflows detected in other ULIRGs (10²-10³ M_⊙ yr⁻¹; e.g. Rupke et al. 2005a,b). We estimate that the total mass in the warm gas outflow is $M_{outflow} = (8^{+3}_{-2}) \times 10^5$ M_⊙ with filling factors³ of $\epsilon = (4.4^{+1.8}_{-1.5}) \times 10^{-4}$ and $\epsilon = (1.6^{+0.7}_{-0.5}) \times 10^{-7}$ for the regions emitting the broad and very broad components respectively.

In order to gauge the impact of the warm gas outflow on the circumnuclear gas, it is important to estimate the

kinetic power of the outflow, including both the radial and turbulent components in the gas motion. Assuming that the relatively large linewidth of the outflowing gas reflects a turbulent motion that is present at all locations in the outflow region, the kinetic power is:

$$\dot{E} = 6.34 \times 10^{35} \frac{\dot{M}}{2} (v_{out}^2 + (\text{FWHM})^2 / 1.85) \text{ erg s}^{-1} \quad (2)$$

where FWHM is the full width at half maximum of the [OIII] line component in km s⁻¹, and \dot{M} is the mass outflow rate expressed in solar masses per year. The kinetic powers are $\dot{E} = (2.3 \pm 0.9) \times 10^{42}$ erg s⁻¹ and $\dot{E} = (1.1^{+0.6}_{-0.4}) \times 10^{42}$ erg s⁻¹ for the broad and very broad components. Hence, the total kinetic power in the warm gas outflow is $\dot{E} = (3.4^{+1.5}_{-1.3}) \times 10^{42}$ erg s⁻¹.

Combining the kinetic power with the bolometric luminosity provides an estimate of the fraction of the total available power from accretion onto the black hole driving the outflows. Dasyra et al. (2006) publish two black hole mass estimates for the active western nucleus of PKS 1345+12, one derived using $M_{BH} - \sigma$ as $M_{BH} = 6.54 \times 10^7$ M_⊙ (Dasyra et al. 2006), and a smaller mass estimate of $M_{BH} = 1.75 \times 10^7$ M_⊙ based on the assumption that $\frac{1}{2}L_{FIR} = L_{bol} = L_{Edd}$ ⁴. Comparing the two black hole masses gives an idea of the Eddington ratio:

$$\frac{M_{BH,FIR}}{M_{BH,dyn}} = \frac{L_{bol}}{L_{Edd}} = 0.27 \quad (3)$$

This estimate for the Eddington ratio is reasonable. For the similar source PKS 1549-79, Holt et al. (2006) derived Eddington ratios in the range $0.3 < L_{bol} < 57$ depending on the black hole mass used. Furthermore, Wu (2009) collated data from the literature for a large sample of compact radio sources. Of the 51 sources with quoted L_{bol}/L_{Edd} ⁵, the Eddington ratio is typically high ($10^{-2} < L_{bol}/L_{Edd} < \text{several}$) compared to samples of radio loud and radio quiet quasars and broad line radio galaxies (typically $L_{bol}/L_{Edd} < 0.1$; e.g. Dunlop et al. 2003; Marchesini et al. 2004) but similar to the ratios observed in narrow line seyfert Is ($L_{bol}/L_{Edd} = 0.16$; Bian et al. 2008); with $L_{bol}/L_{Edd} = 0.28$ and $L_{bol}/L_{Edd} = 0.26$ for the CSS and GPS sources respectively. The estimate of $L_{bol}/L_{Edd} = 0.27$ for PKS 1345+12 derived from the ratio of the two black hole estimates is therefore entirely consistent with other GPS sources where this ratio is known with more certainty.

With this in mind, we calculate the fraction of the accretion power in the outflow as: $\dot{E}/L_{bol} = (1.3 \pm 0.2) \times 10^{-3}$. Hence, if the assumed bolometric luminosity conversion is correct, only a small fraction of the available accretion power is driving the warm gas outflow. This is similar to

⁴ It is also possible to estimate the bolometric luminosity from the extinction-corrected [O III] emission line luminosity using the conversion factors given in Lamastra et al. (2009). Our reddening corrected total [O III] luminosity is $L_{[OIII]} = (2.11 \pm 0.25) \times 10^{43}$ erg s⁻¹ and corresponds to a bolometric luminosity of $L_{[OIII]} = (9.5 \pm 1.1) \times 10^{45}$ erg s⁻¹, which is similar to the estimate derived from the FIR luminosity.

⁵ Whilst PKS 1345+12 is included in the paper, Wu (2009) did not include the estimate of L_{bol}/L_{Edd} from Dasyra et al. (2006), which is expanded for clarity above.

³ See equation 3 in Holt et al. (2008).

the findings for another compact radio source, PKS 1549-79 (Holt et al. 2006). This is in stark contrast to the requirements of the majority of quasar feedback models which require a much larger fraction of the accretion power of the black hole ($\sim 5\text{--}10\%$ of L_{bol}) to be thermally coupled to the circumnuclear gas, but similar to the recent work of Hopkins & Elvis (2010).

It is also unlikely that the warm gas outflow is capable of removing all the warm/cool gas from the central regions of the host galaxy by itself. If we assume that PKS1345+12 has a total mass $M_{\text{total}} \sim 10^{11} M_{\odot}$, and a gas mass $M_{\text{gas}} \sim 10^{10} M_{\odot}$ contained within a radius of 5 kpc – conservative assumptions for ULIRGs which are likely to have a larger gas mass concentrated within a smaller radius – the gravitational binding energy of the gas is $E_{\text{bind}} \approx GM_{\text{gas}}M_{\text{total}}/R_{\text{gas}} \approx 2 \times 10^{58}$ erg. In comparison, the warm gas outflow will deposit only $\sim 10^{56}$ erg into the surrounding ISM, assuming that it can persist in its current form for the typical 10^7 yr lifetime of an extragalactic radio source. Again, these observations are consistent with the limits calculated for another compact (young) radio source PKS 1549-79 (H06). This result may suggest that PKS1345+12 will grow into a large radio galaxy in a gas-rich host. However, with its double nucleus, PKS 1345+12 is still in the pre-coalescence stage of the merger, observed during the first peri-centre passage, but immediately before (within ~ 0.1 Gyr) of the coalescence of the nuclei (Tadhunter et al. 2010). According to the merger simulations, PKS 1345+12 is therefore yet to pass through the most active phase (both in terms of nuclear activity and star formation) of the merger when the nuclei coalesce. An increase in nuclear activity may increase the strength of the winds/outflows and an increase in star formation will also consume large quantities of the ambient ISM. It is therefore unclear whether or not PKS 1345+12 is a progenitor of a gas rich radio galaxy.

It is clear that the kinetic power of the warm gas outflow in PKS 1345+12 is significantly less than that required by the majority of current quasar feedback models. Could this be because we have not accurately measured all of the input parameters or made inaccurate assumptions? In the above analysis, the key observable parameters are the electron density, the size of the outflow region, the luminosity of the $H\beta$ line and the black hole parameters (black hole mass and the Eddington ratio). Following through, an underestimate of the kinetic power, \dot{E} , would result from an overestimated electron density and/or outflowing region size, or from an underestimated $H\beta$ luminosity. Furthermore, if the black hole mass and/or the bolometric luminosity is overestimated, the impact of the outflow may be underestimated.

We are confident that the size of the outflowing region has not been overestimated as recent high-resolution HST imaging of PKS 1345+12 have shown the optical line emission to be on a similar scale to the compact radio emission (Batcheldor et al. 2007). If anything, the outflowing region may be significantly larger if projection effects are important.

The electron density derived by this new technique is high ($N_e \sim 10^{4-5} \text{ cm}^{-3}$) and therefore one to two orders of magnitude above typical NLR densities in the literature measured using traditional diagnostics. As discussed in Section 3.3, the large uncertainties in the reddening estimate will have a significant effect on the line ratios. However, as

demonstrated by Figure 3, even with large changes in the reddening for the very broad component, the derived density remains unchanged. Despite this, it is still important to consider whether such high densities are realistic and what effect this has on our overall conclusions.

Whilst it is possible the new technique overestimates the density, very high densities are not surprising; high gas densities have been observed in a number of compact radio sources (Holt et al. 2009) and the original study of PKS 1345+12 using the $[S \text{ II}]6716/6731$ ratio calculated a relatively high lower limit ($N_e \gtrsim 5 \times 10^3 \text{ cm}^{-3}$; H03). Furthermore, large quantities of gas in the nuclear regions of PKS 1345+12 have been observed in a variety of wavebands (see Section 1). Using the lower limit for the electron density provides upper limits for the mass outflow rate ($\dot{M} < 21 M_{\odot} \text{ yr}^{-1}$), the kinetic power ($\dot{E} < 3.8 \times 10^{43} \text{ erg s}^{-1}$) and the fraction of the available accretion power in the outflow ($\dot{E}/L_{\text{Edd}} < 4 \times 10^{-3}$). Hence, even if our electron density is overestimated by as much as two orders of magnitude, the amount of energy in the outflow is still significantly lower than the required 5-10%.

It is possible that the errors on the derived $H\beta$ luminosities are large. As discussed above, the nuclear regions of PKS 1345+12 are known to contain large quantities of gas and dust. The optical emission line components are known to be heavily extinguished (H03 and Section 3.3), whilst radio and X-ray studies detect large absorbing columns: $N_{\text{H}} > 10^{22} \text{ cm}^{-2}$ (radio; Morganti et al. 2005) and $N_{\text{H}} = 2.3 \times 10^{22} \text{ cm}^{-2}$ (X-ray; Siemiginowska priv. comm.). However, as demonstrated in Section 3.3, it is difficult to constrain the degree of reddening, although all estimates discussed in Section 3.3 do agree within the (large) errors. Above, we calculated the various outflow properties, such as mass outflow rates and kinetic powers, based on the $H\beta$ luminosities derived from the new $H\beta$ flux measurements from the VLT spectra, and the reddening estimates derived from the diagnostic diagram in Figure 3. We now calculate the same quantities using the new $H\beta$ fluxes and the original reddening estimates from H03 in order to understand the possible uncertainties in our results.

In short, for this case, we calculate the following: (i) mass outflow rates of $\dot{M}_{\text{B}} = 2.7 M_{\odot} \text{ yr}^{-1}$ and $\dot{M}_{\text{VB}} = 7.2 M_{\odot} \text{ yr}^{-1}$ with a total mass outflow rate of $\dot{M}_{\text{total}} = 9.9 M_{\odot} \text{ yr}^{-1}$; (ii) volume filling factors of $\epsilon_{\text{B}} = 1.7 \times 10^{-4}$ and $\epsilon_{\text{VB}} = 1.9 \times 10^{-6}$; (iii) total gas mass of $M_{\text{total}} = 8 \times 10^5 M_{\odot}$; (iv) kinetic powers of $\dot{E}_{\text{B}} = 8.7 \times 10^{41} \text{ erg s}^{-1}$ and $\dot{E}_{\text{VB}} = 1.4 \times 10^{43} \text{ erg s}^{-1}$ with a total kinetic power of $\dot{E}_{\text{total}} = 1.5 \times 10^{43} \text{ erg s}^{-1}$; (v) fraction of the total available accretion in the warm outflow: $\dot{E}/L_{\text{Edd}} = 6 \times 10^{-3}$. Hence, implementing the original reddening estimate from H03 rather than those derived from Figure 3 decreases the impact of the broad component by a factor of ~ 3 , but boosts the impact of the very broad component by a factor of ~ 12 . Overall, this increases the total impact of the outflow by a factor of 4.6, from 0.13% of L_{bol} to 0.6% of L_{bol} and demonstrates that our results are robust against large variations in the reddening.

The final possible source of uncertainties relates to the black hole properties, namely the mass, the bolometric and Eddington luminosities and the Eddington ratio. In the above calculations, we have followed Dasyra et al. (2006) and assumed that $\frac{1}{2}L_{\text{FIR}} = L_{\text{bol}} = L_{\text{Edd}}$ provides a good

estimate of the bolometric luminosity. Whilst this conversion may be a good general assumption, in highly complex sources like PKS 1345+12, the FIR emission is likely to contain many components. We have also compared the black hole masses in Dasyra et al. (2006) and estimated an Eddington ratio of 0.27. To quantify the possible errors on our result, we take the extreme case and assume that PKS 1345+12 is accreting at the Eddington ratio, with the larger of the two black hole masses. In this case, we calculate $\dot{E}/L_{\text{Edd}} = (3.6 \pm 0.16) \times 10^{-4}$. Hence, potential errors in the black hole mass are likely to reduce the impact of the outflow.

Given the above, as suggested for a similar source PKS 1549-79 by Holt et al. (2006), it is likely that the warm gas outflow detected in the optical emission lines accounts for only a small fraction of the total outflow with the remaining mass in hotter or cooler phases of the ISM. Indeed Morganti et al. (2005) reported the discovery of massive neutral outflows in a sample of 7 compact radio sources which includes PKS 1345+12. The HI outflow in PKS 1345+12 is: $\dot{M} \sim 8 - 21 \text{ M}_{\odot} \text{ yr}^{-1}$, with the lower end of the range similar to that for the warm gas outflow. Taking this range of mass outflow rates, and assuming the outflow velocity and FWHM to be 600 km s^{-1} (i.e. FWZI/2; Morganti priv. comm.), we find the HI outflow has a kinetic power of $1 \times 10^{42} \lesssim \dot{E} \text{ (erg s}^{-1}\text{)} \lesssim 4 \times 10^{42}$ which accounts for $4 \times 10^{-4} \lesssim \dot{E}/L_{\text{bol}} \lesssim 1 \times 10^{-3}$ of the available accretion energy.

Combining the HI and optical results, the total observed outflow is currently of the order of $16\text{--}29 \text{ M}_{\odot} \text{ yr}^{-1}$, with a kinetic power of $4.4 \times 10^{42} < \dot{E} < 7.4 \times 10^{42} \text{ erg s}^{-1}$ and accounts for 0.2-0.3% of the available accretion energy, L_{bol} .

It is also interesting to consider the amount of energy locked into the radio emission by comparing the radio power, Q_{jet} , to the accretion energy. Taking the radio jet power calculated by Wu (2009) of $\log(Q_{\text{jet}}) = 44.62^6$ and the above bolometric luminosity, we find $Q_{\text{jet}}/L_{\text{bol}} = 0.16$. In other words, around 16 per cent of the total available accretion power is currently powering the radio jets. Whilst there is various evidence to suggest that the HI and optical emission line outflows are driven by the radio jets (e.g. high outflow velocities e.g. Holt et al. 2008; co-spatial radio and optical emission on similar scales in GPS and CSS sources and in some CSS sources, evidence for radio-optical alignment e.g. de Vries et al. 1999; Axon et al. 2000; O’Dea et al. 2002; Labiano et al. 2005; Batcheldor et al. 2007; Privon et al. 2008), it appears that the mechanical coupling of the radio jet to the ISM is relatively inefficient.

PKS 1345+12 is also detected in X-rays (e.g. O’Dea et al. 2000; Siemiginowska et al. 2008) with a soft X-ray excess ($L(0.5\text{--}2\text{keV}) = 2 \times 10^{42} \text{ ergs sec}^{-1}$) and a harder X-ray spectrum than typical for AGN (Siemiginowska priv. com.). The emission has two clear features: i) an extended ($\sim 15 \text{ kpc}$) diffuse component, which may be the result of thermal emission in the host galaxy, and ii) an elongated feature to the SW of the active nucleus, which appears to be closely related to the VLBI radio source. Further observations are required to establish whether a hot gas outflow is present in PKS 1345+12.

To summarise, after consideration of all possible sources of error, the most extreme kinetic power we calculate is still at least an order of magnitude smaller than that currently required by the majority of galaxy evolution models but similar to the energy requirements suggested by recent work on a two-phase feedback model (Hopkins & Elvis 2010).

4.2 PKS 1345+12 – a young radio source?

It is now well accepted that compact (GPS and CSS) radio sources are compact due to evolutionary stage rather than due to the effects of frustration by a dense ISM (e.g. Fanti et al. 1995). However, recent simulations of radio jet-ISM interactions have shown that, if the ISM forms dense clouds, much smaller masses could significantly disrupt the propagation of the jet. For example, jet interactions with dense clouds (e.g. of the order $M_{\text{gas}} \sim 10^6 \text{ M}_{\odot}$) may be significantly disrupted (e.g. Sutherland & Bicknell 2007) compared to the much larger gas masses required ($M_{\text{gas}} \sim 10^{9\text{--}11} \text{ M}_{\odot}$) required if the gas is distributed in a homogeneous or clumpy distribution (e.g. De Young 1993; Carvalho 1994, 1998).

We have seen that the nuclear regions of PKS 1345+12 harbour a rich, dense ISM, but is there sufficient mass to confine and frustrate the radio source?

In our original study in 2003, using the following equation:

$$M_{\text{gas}} = m_p \frac{L(\text{H}\beta)}{N_e \alpha_{\text{H}\beta}^{\text{eff}} h\nu_{\text{H}\beta}} \quad (4)$$

we derived limits on the gas mass for PKS 1345+12 of: $M_{\text{gas}} > 2.61 \times 10^5 \text{ M}_{\odot}$, $M_{\text{gas}} < 0.92 \times 10^5 \text{ M}_{\odot}$ and $M_{\text{gas}} < 5.64 \times 10^5 \text{ M}_{\odot}$ in the regions emitting the narrow, broad and very broad components respectively; with an upper limit of order 10^6 M_{\odot} for the total mass of line emitting gas in the kinematically disturbed emission line components.

Using the new gas densities and H β luminosities measured in this paper, we now derive gas masses of: $M_{\text{gas}} = (1.2_{-0.4}^{+0.3}) \times 10^5 \text{ M}_{\odot}$, $M_{\text{gas}} = (7.7_{-2.6}^{+3.1}) \times 10^5 \text{ M}_{\odot}$ and $M_{\text{gas}} = (2.9_{-0.6}^{+1.0}) \times 10^4 \text{ M}_{\odot}$ for the narrow, broad and very broad components respectively. This gives a total gas mass of $(9.2_{-3.0}^{+3.4}) \times 10^5 \text{ M}_{\odot}$ with $(8 \pm 3) \times 10^5 \text{ M}_{\odot}$ in the outflowing components.

H03 discussed that, even with the original estimate of $< 10^6 \text{ M}_{\odot}$, it was unlikely that there was sufficient *warm* gas in the nuclear regions of PKS 1345+12 to confine and frustrate the young, expanding radio jets and only the presence of dense clouds would be able to significantly disrupt the propagation of the jet. The newly derived gas densities suggest the *warm* gas mass is one-two orders of magnitude smaller than the previously calculated limit. It is therefore unlikely that the propagation of the radio jets in PKS 1345+12 will be significantly affected by the *warm* ISM in this source. However, it should be noted that much higher gas masses have been measured in e.g. molecular gas ($3.3 \times 10^{10} \text{ M}_{\odot}$; Evans et al. 1999).

5 CONCLUSIONS AND FUTURE WORK

Using new, deep VLT/FORS spectra of the young radio source PKS 1345+12, we have piloted a new technique using

⁶ At 178MHz.

the transauroral [S II] and [O II] emission lines to determine the electron density in a source where the highly broadened and complex emission line ratios precluded measurements using the traditional diagnostics (e.g. [S II]6716/6731). Our observations reveal that the outflowing warm gas in this compact radio source is dense ($N_e \sim 10^{4-5} \text{ cm}^{-3}$). In addition to previous issues regarding the modelling of [S II]6716,6731 doublet, this shows that the electron densities in this source are much higher than the range of densities to which the diagnostic is sensitive.

The newly determined electron densities have enabled us to calculate key parameters for determining the impact of the fast, warm outflow in this source (mass outflow rate, kinetic power). Whilst at face value the warm gas outflow appears extreme, with outflow velocities of up to 2000 km s⁻¹, the outflow is driven by only a small fraction of the energy available from accretion power. Comparisons with the majority of AGN feedback models in the literature suggest that the outflow in PKS 1345+12 is at least an order of magnitude smaller than required. However, recent work by Hopkins & Elvis (2010) suggests that with a two-stage feedback model, the initial feedback requirements may be similar to what is observed in PKS 1345+12.

ACKNOWLEDGEMENTS

Based on observations collected at the European Southern Observatory, Chile (078.B-0537). JH acknowledges financial support from NWO. We thank Prof. S. Veilleux for making the near-IR spectrum available to us. We thank Dr. C. Booth for useful discussions regarding AGN feedback theory.

REFERENCES

- Axon D. J., Capetti A., Fanti R., Morganti R., Robinson A., Spencer R., 2000, *AJ*, 120, 2284
- Batcheldor D., Tadhunter C. N., Holt J., Morganti R., O'Dea C. P., Axon D. J., Koekemoer A., 2007, *ApJ*, 661, 70
- Benson A. J., Bower R. G., Frenk C. S., Lacey C. G., Baugh J. L., Cole S., 2003, *ApJ*, 599, 38
- Bian W.-H., Hu C., Gu Q.-S., Wang J.-M., 2008, *MNRAS*, 390, 752
- Booth C. M., Schaye J., 2009, *MNRAS*, 398, 53
- Carvalho J. C., 1994, *A&A*, 292, 392
- Carvalho J. C., 1998, *A&A*, 329, 845
- Cattaneo A., Faber S. M., Binney J., Dekel A., Kormendy J., Mushotzky R., Babul A., Best P. N., Brggen M., Fabian A. C., Frenk C. S., Khalatyan A., Netzer H., Mahdavi A., Silk J., Steinmetz M., Wisotzki L., 2009, *Nat*, 460, 213
- Dasyra K. M., Tacconi L. J., Davies R. I., Genzel R., Lutz D., Naab T., Burkert A., Veilleux S., Sanders D. B., 2006, *ApJ*, 638, 745
- de Vries W. H., O'Dea C. P., Baum S. A., Barthel P. D., 1999, *ApJ*, 526, 27
- De Young D. S., 1993, *ApJ*, 402, 95
- Di Matteo T., Springel V., Hernquist T., 2005, *Nat*, 433, 604
- Dickson R. D., Tadhunter C. N., Shaw M., Clark N., Morganti R., 1995, *MNRAS*, 273, 29
- Dunlop J. S., McLure R. J., Kukula M. J., Baum S. A., O'Dea C. P., Hughes D. H., 2003, *MNRAS*, 340, 1095
- Evans A. S., Kim D. C., Mazzarella J. M., Scoville N. Z., Sanders D. B., 1999, *ApJ*, 521, L107
- Fabian A. C., 1999, *MNRAS*, 308, L39
- Fanti C., Fanti R., Schilizzi R. T., Spencer R. E., Stanghellini C., 1995, *A&A*, 302, 317
- Ferrarese L., Merritt D., 2000, *ApJ*, 539, 9
- Gebhardt K., Kormendy J., Ho L. C., Bender R., Bower G., Dressler A., Faber S. M., Filippenko A. V., Green R., Grillmair C., Lauer T. R., Magorrian J., Pinkey J., Richstone D., Tremaine S., 2000, *ApJ*, 539, 13
- Holt J., Tadhunter C. N., González Delgado R. M., Inskip K. J., Rodriguez Zaurin J., Emonts B. H. C., Morganti R., Wills K. A., 2007, *MNRAS*, 381, 611
- Holt J., Tadhunter C. N., Morganti R., 2003, *MNRAS*, 342, 227
- Holt J., Tadhunter C. N., Morganti R., 2008, *MNRAS*, 387, 197
- Holt J., Tadhunter C. N., Morganti R., 2009, *MNRAS*, 400, 589
- Holt J., Tadhunter C. N., Morganti R., Bellamy M. J., González Delgado R. M., Tzioumis A., Inskip K. J., 2006, *MNRAS*, 370, 1633
- Hopkins P. F., Elvis M., 2010, *MNRAS*, 401, 7
- Kurosawa R., Proga D., Nagamine K., 2009, *ApJ*, 707, 823
- Labiano A., P. O. C., Gelderman R., de Vries W. H., Axon D. J., Barthel P. D., Baum S. A., Capetti A., Fanti R., Koekemoer A. M., Morganti R., Tadhunter C. N., 2005, *A&A*, 436, 493
- Lamastra A., Bianchi S., Matt G., Perola G. C., Barcons X., Carrera F. J., 2009, *A&A*, 504, 73
- Marchesini D., Celotti A., Ferrarese L., 2004, *MNRAS*, 351, 733
- Marconi A., Hunt L. K., 2003, *ApJ*, 589, L21
- Morganti R., Tadhunter C. N., Oosterloo T. A., 2005, *A&A*, 444, L9
- O'Dea C. P., 1998, *PASP*, 110, 493
- O'Dea C. P., de Vries W. H., Koekemoer A. M., Baum S. A., Morganti R., Fanti R., Capetti A., Tadhunter C. N., Barthel P. D., Axon D. J., Gelderman R., 2002, *AJ*, 123, 2333
- O'Dea C. P., de Vries W. H., Worrall D. M., Baum S. A., Koekemoer A., 2000, *AJ*, 119, 478
- Osterbrock D. E., 1989, in *Astrophysics of Gaseous Nebulae and Active Galactic Nuclei* University Science Books, California, pp 61–62
- Osterbrock D. E., Fulbright J. P., Keane M. J and Trager S. C., 1996, *PASP*, 108, 277
- Privon G. C., O'Dea C. P., Baum S. A., Axon D. J., Kharb P., Buchanan C. L., Sparks W., Chiaberge M., 2008, *ApJS*, 175, 423
- Rodriguez Zaurin J., Holt J., Tadhunter C. N., González Delgado R. M., 2007, *MNRAS*, 375
- Rupke D. S., Veilleux S., Sanders D. B., 2005a, *ApJ*, 632, 751
- Rupke D. S., Veilleux S., Sanders D. B., 2005b, *ApJS*, 160, 115
- Schneider D. P. e. a., 2010, *ApJ*, in press
- Seaton M. J., 1979, *MNRAS*, 187, 73P
- Siemiginowska A., La Massa S., Aldcroft T. L., Bechtold J., Elvis M., 2008, *ApJ*, 684, 811

- Silk J., Rees M. J., 1998, *A&A*, 331, L1
- Smith E. P., Heckman T. P., 1989, *ApJS*, 69, 365
- Spoon H. W. W., Holt J., 2009, *ApJ*, 702, 42
- Springel V., di Matteo T., Hernquist L., 2005, *MNRAS*, 361, 776
- Stanghellini C., O’Dea C. P., Baum S. A., Laurikainen E., 1993, *ApJS*, 388, 1
- Sutherland R. S., Bicknell G. V., 2007, 173, 37
- Tadhunter C. N., Holt J., González Delgado R., Rodríguez Zaurín J., Villar-Martín M., Morganti R., Emonts B. H. C., Ramos Almeida C., Inskip K. J., 2010, *MNRAS*, submitted
- Tadhunter C. N., Robinson T. G., González Delgado R. M., Wills K., Morganti R., 2005, *MNRAS*, 356, 480
- Tadhunter C. N., Shaw M. A., Morganti R., 1994, *MNRAS*, 271, 807
- Tremaine S., Gebhardt K., Bender R., Bower G., Dressler A., Faber S. M., Filippenko A. V., Green R., Grillmair C., Ho L. C., Kormendy J., Lauer T. R., Magorrian J. & Pinkney J., Richstone D., 2002, *ApJ*, 574, 740
- Veilleux S., Cecil G., Bland-Hawthorn J., 2005, *ARA&A*, 43, 769
- Wild V., Heckman T., Charlot S., 2010, *astro-ph/1002.3156*
- Wu Q. W., 2009, *MNRAS*, 398, 1905